

Impact of strain-induced electronic topological transition on the thermoelectric properties of PtCoO_2 and PdCoO_2

Markus Ernst Gruner^{1,2,*}, Ulrich Eckern³, and Rossitza Pentcheva²

¹*Forschungs-Neutronenquelle Heinz Maier-Leibnitz (FRM II),
Technische Universität München, 85748 Garching, Germany*

²*Faculty of Physics and Center for Nanointegration, CENIDE,
University of Duisburg-Essen, 47048 Duisburg, Germany and*

³*Institute of Physics, University of Augsburg, 86135 Augsburg, Germany*
(Dated: December 1, 2015)

By a combination of first-principles calculations and semi-classical Boltzmann transport theory, we investigate the effect of epitaxial strain on the electronic structure and transport properties of PtCoO_2 and PdCoO_2 . In contrast to the rather uniform elastic response of both systems, we predict for PtCoO_2 a high sensitivity of the out-of-plane transport properties to strain, which is not present in PdCoO_2 . At ambient temperature, we identify a considerable absolute change in the thermopower from $-107 \mu\text{V/K}$ at -5% compressive strain to $-303 \mu\text{V/K}$ at $+5\%$ tensile strain. This remarkable response is related to distinct changes of the Fermi surface, which involve the crossing of two additional bands at a moderate compressive in-plane strain. Combining our transport results with available experimental data on electrical and lattice thermal conductivity we predict a thermoelectric figure of merit of up to $ZT = 0.25$ at $T = 600 \text{ K}$ for strained PtCoO_2 .

I. INTRODUCTION

Recently, the quest for new thermoelectric materials beyond Bi_2Te_3 has gained considerable momentum which is owed to the increasing need of highly performing materials for energy harvesting and conversion. The most promising materials classes identified so far are found among the semiconductors, which allow a careful adjustment of charge carrier type and concentration in order to achieve the optimum balance between thermopower, electrical, and thermal conductivity.^{1,2} Together with the idea to exploit low-dimensional quantum-well structures to increase the thermoelectric performance,³ this leads to a series of new high performance materials which are formed of heterostructures or quantum dot superlattices.⁴⁻⁶ Oxides, such as Na_xCoO_2 -type or $\text{Ca}_3\text{Co}_4\text{O}_9$,⁷⁻¹¹ represent another promising materials class with the advantage of non-toxicity and abundance of their components in combination with the chemical and thermal stability rather than record-breaking performance values.

Low-dimensionality is readily realized in naturally layered structures, which are for instance found in a specific class of cobaltates, the delafossites. Among those hexagonal ABO_2 compounds, PdCoO_2 and PtCoO_2 take a special position, since these are – unlike most of the oxides, which are semiconducting or insulating – very good metallic conductors.¹²⁻¹⁴ Such a material usually disqualifies for thermoelectric applications,¹ but it was discovered early that the conductivity of PdCoO_2 and PtCoO_2 is highly anisotropic.^{12,15} Recent theoretical work^{16,17} reports also a qualitative difference in the thermoelectric properties with respect to transport within the a - b plane and along the hexagonal c -axis. The calculations predict significant negative values of about $-100 \mu\text{V K}^{-1}$ (PdCoO_2) and $-250 \mu\text{V K}^{-1}$ (PtCoO_2) for the out-of-plane component of the thermopower at room tempera-

ture, in contrast to moderate $+5 \mu\text{V K}^{-1}$ in-plane.¹⁷ Such a large anisotropy in the thermopower can give rise to a considerable laser induced voltage, which can be exploited to design photosensors based on the transverse thermoelectric effect.¹⁸

Both compounds are stable and have been synthesized as high quality single crystals employing the so-called methathetical reaction.^{15,19-22} In PtCoO_2 and PdCoO_2 , the Co ion is found in the trivalent Co^{3+} state, which shows a $S=0$ low spin configuration, while Pd and Pt are monovalent.^{20,23-26} Experiment^{23,26-28} and first principles theory^{16,29-31} show consistently that the Fermi level of PdCoO_2 is populated by Pd states, while oxygen states are scarce and Co states are essentially absent. Photoemission spectroscopy confirms the validity of this picture also for PtCoO_2 .²⁴ Thus the high in-plane conductivity arises from the hybridized noble metal 4d and 5s electrons which contribute states at the Fermi level, whereas the CoO_6 octahedra can be thought to form an insulating layer, inhibiting transport along the perpendicular z -axis. The absence of hybridized Co states at the Fermi level results in a quasi-two-dimensional electronic arrangement. This is mirrored by a Fermi-surface, which shows nearly no dispersion along k_z and thus has a quasi two-dimensional shape.^{16,17,30,32} In consequence, the Fermi velocities, i. e., the gradients of k -resolved band structure at E_F , are restricted to the x - y plane, while the rather flat Fermi surface along k_z prevents a significant contribution to the out-of-plane conductivity σ_{zz} . The predicted cross-section of the Fermi surface in the shape of a closed hexagon was validated by Noh *et al.*³² based on angular-resolved photoemission spectroscopy (ARPES).

In the present work, we consider PdCoO_2 and PtCoO_2 as an intrinsically layered system serving as a simple prototype of a heterostructure considered for future thermoelectric applications. We determine the dependence

of the electronic structure on epitaxial in-plane strain by means of first-principles calculations. Using this as input, we obtain the transport properties in the framework of semi-classical Boltzmann transport theory in the constant relaxation time approximation. We identify a remarkable dependence of the electronic transport of PtCoO_2 on epitaxial strain, which stands in clear contrast to the rather uniform strain response of the elastic properties. We will show that this stunning discrepancy is related to an *electronic topological transition*, which, in turn, is beneficial in improving the thermoelectric performance of the material. It manifests in a variation of the out-plane thermopower by a factor of three and the out-of-plane conductivity by more than one order of magnitude.

After a short survey of the computational details in Sec. II, we will shortly review the similarities in the structural behavior of epitaxially strained PtCoO_2 and PdCoO_2 in Sec. III A. The different strain response of the electronic structure is explained in Sec. III B, while Sec. III C is devoted to the immediate consequences for in-plane and out-of-plane conductivity. Thermopower and a prediction for the thermoelectric figure of merit for the strained materials are presented in Sec. III D.

II. NUMERICAL DETAILS

The electronic structure was investigated within the framework of density functional theory (DFT) employing the Vienna ab initio Simulation package (VASP),^{33,34} which uses a plane wave basis set for the description of the valence electrons in combination with the projector augmented wave approach (PAW).³⁵ In our calculations, we considered explicitly the $2s^2 2p^4$ electrons for O, $3d^8 4s^1$ for Co, $4p^6 4d^9 5s^1$ for Pd and $5d^9 6s^1$ for Pt, choosing a cutoff energy of 500 eV. The exchange-correlation part of the Hamiltonian was represented by the generalized gradient approximation (GGA) of Perdew, Burke and Ernzerhof.³⁶

The response of the system to epitaxial strain exerted along the a - b -plane was calculated from the hexagonal 12 atom unit cell within the scalar-relativistic approximation. The hexagonal basis of this cell allows a straightforward manipulation of the lattice parameters according to the epitaxial constraint. For a given value of a , the c lattice parameter and atomic positions were optimized for minimum energy modelling the epitaxial constraint. In order to obtain accurate eigenvalues, as needed for the transport calculations described below, we transformed the 12 atom unit cell with hexagonal basis to the 4 atom primitive cell with rhombohedral basis using a mesh of $41 \times 41 \times 41$ k -points. We included the spin-orbit term to the Hamiltonian in our self-consistent treatment, which yields small but noticeable changes to the results. For additional corroboration and high quality Fermi surfaces, parts of the calculations were repeated with the full-potential augmented plane wave method

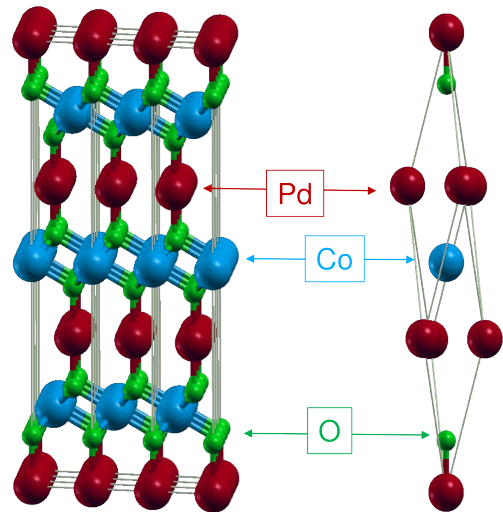


FIG. 1: (color online) Representation of PdCoO_2 and PtCoO_2 delafossites in a unit cell with 12 atoms corresponding to the hexagonal basis (left image, 3 times replicated in a and b direction) and a four-atom rhombohedral primitive cell (right).

Wien2k.³⁷ Thermoelectric properties at finite temperatures were obtained in the framework of semiclassical Boltzmann transport theory in the constant relaxation time approximation under the constraint of a conserved number of carriers. This step was carried out with the BoltzTraP³⁸ code based on the eigenvalues obtained from our VASP calculations. In order to test the effect of additional correlation on the electronic structure and transport properties, we applied the GGA+ U scheme in the rotationally invariant formulation of Dudarev *et al.*³⁹ on the Co d states for selected cases, using different values of $U - J$ up to 5 eV. Further technical details can be found in the supplementary material.⁴⁰

III. RESULTS AND DISCUSSION

A. Structural properties strained PdCoO_2 and PtCoO_2

The delafossites crystallize in a hexagonal structure (see Fig. 1), which can be described by the rhombohedral space group 166 with symmetry $R\bar{3}m$. Pt or Pd are found on the (1a) site at $(0,0,0)$, Co on the (1b) site at $(0,0,1/2)$ and the two oxygen on the (2c) site at $(0,0,\pm u)$, with u as an internal structural parameter. This results in a naturally layered arrangement, consisting of layers of corner-sharing CoO_6 octahedra and linear O-Pd-O or, respectively, O-Pt-O dumbbells. The Pd/Pt atoms form a hexagonal layer with the triangular faces of the CoO_6 octahedra on top of the triangular facets of the Pd/Pt, such that the edge oxygen of CoO_6 become part of the dumbbells.

We find the ground state of both delafossites at

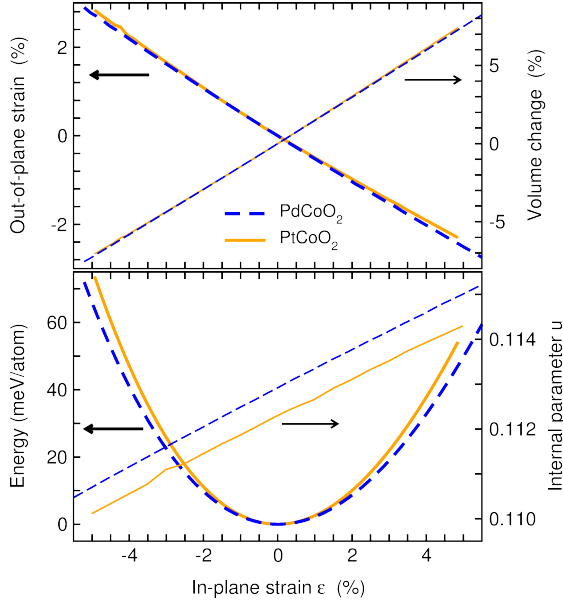


FIG. 2: (color online) Comparison of total energy (bottom graph, left axis), internal parameter u (bottom graph, right axis), out-of-plane strain (top graph, left axis) and unit cell volume (top graph, right axis) relative to the respective bulk equilibrium value as a function of the relative in-plane strain for PdCoO₂ (dark blue color) and PtCoO₂ (bright orange color) obtained from our first-principles calculations.

nearly the same lattice parameters, i.e., $a = 2.870 \text{ \AA}$ and $c = 17.94 \text{ \AA}$ for PdCoO₂ and $a = 2.861 \text{ \AA}$ and $c = 17.95 \text{ \AA}$ for PtCoO₂. Consequently, the atomic volume of the Pd-compound is with $V = 10.66 \text{ \AA}^3/\text{atom}$ slightly larger than the volume of the Pt-compound ($V = 10.61 \text{ \AA}^3/\text{atom}$). These values agree well with previous DFT investigations^{30,41} and experiment ($a = 2.83 \text{ \AA}$ for both compounds),^{20–22,42,43} with the typical overestimation of the lattice constant by approximately one percent as a consequence of the use of the GGA for the exchange-correlation potential. Both systems show an essentially identical response to epitaxial strain. The lower panel of Fig. 2 indicates that epitaxial growth with in-plane strains along a of up to 5% might be realistic, since the corresponding deformation energies are still in the range of typical thermal energies. Applying in-plane strain results in a corresponding opposite strain of the out-of-plane lattice parameter c , which is, however, approximately only half as large. This has the consequence that upon straining the system by $\epsilon = \Delta a/a = \pm 4\%$ the equilibrium volume changes significantly by $\Delta V/V = \pm 5\%$. The increase of c/a with decreasing volume is consistent with pressure experiments on PdCoO₂.⁴² Epitaxial strain also causes a variation of the internal parameter u , which determines the oxygen position relative to the other ions. At equilibrium conditions, we find $u = 1.1129$ for PdCoO₂ and $u = 1.1123$ for PtCoO₂. This corresponds to a Pd-O distance of 2.026 \AA

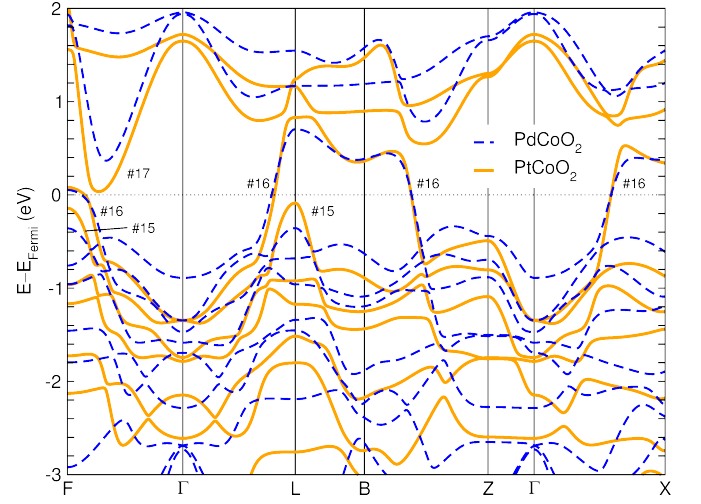


FIG. 3: (color online) Band structure of PtCoO₂ (solid orange line) and PdCoO₂ (dashed blue line) in the vicinity of the Fermi level. The numbers denote the bands close to E_{F} , which are relevant for our discussion. The counting starts from the valence band minimum (core and semicore states such as the Pd $4p^6$ are not considered).

and a Pt-O distance of 2.015 \AA in combination with Co-O distances of 1.917 \AA and 1.919 \AA , respectively. Four percent of tensile strain causes u to increase by approximately 2%. This has an opposite effect on the Co-O distance as compared to the distance between O and the Pt-group metal. For both oxides, the Co-O distance increases by +1.8%, while the distance between O and the noble metal decreases by approximately -0.5% . Under -4% compressive strain, we observe the opposite effect with variations of -1.5% and $+0.6\%$, respectively.

B. Electronic structure and Fermi surface of strained PtCoO₂ and PdCoO₂

The band structure of the unstrained delafossites, compared in Fig. 3, suggests at first sight that the electronic features relevant for the transport properties, which appear close to the Fermi level, E_{F} , are similar for both compounds. In both cases only one band (i.e., the 16th band of valence electrons disregarding the semicore states in counting) is crossing E_{F} which is formed by $d_{3z^2-r^2}$ and s -type orbitals with Pd/Pt character.^{16,29,30} Its rather steep slope in k_x - k_z -direction, which is responsible for the excellent in-plane conductivity, corresponds to a section of a parabolic structure, which has its minimum at Γ at -2.6 eV for PtCoO₂ and -2.3 eV for PdCoO₂ and is intersected by hybridizing bands with d-character several times below E_{F} . Although most other bands of PtCoO₂ are shifted downward due to the larger bandwidth related to the larger extent of the $5d$ shell of Pt compared to the $4d$ electrons of Pd, the 16th band does not change its shape in the immediate vicinity of E_{F} .

This is different for the next lower, completely filled band (i.e., the 15th band), which forms hole pockets in the vicinity of the zone boundary, in particular, near the special points F and L. The next higher unoccupied band (17th band) displays a marked minimum (electron pocket) along Γ -L, which comprises Co e_g states^{29,30} that are absent in the vicinity of E_F otherwise. In PtCoO₂, these features of the 15th and the 17th band come very close to E_F within 100 meV, while in PdCoO₂, they are separated from the Fermi surface by more than 300 meV. As we will show below, these fine details of the electronic structure give rise to qualitatively different transport properties under epitaxial strain which stand in contrast to the rather uniform elastic response of both systems.

The energy minimum along Γ -F in the 17th band might be interpreted as a consequence of the hybridization between the Co $3d_{e_g}$ bands with the parabolic section of the 16th band (see the Co-resolved band structure of PtCoO₂ in Fig. 4d-4f), which manifests in a sharp peak in the electronic density of states 0.4 eV above the Fermi level (see supporting material⁴⁰ and Refs. 29 and 30 for the density of states and orbital resolved band-plots), while the Co $3d_{t_{2g}}$ and the Pd $4d_{xz}$ and $4d_{yz}$ states are located 0.5-2 eV below E_F . In comparison, the hybridization between Pt $5d_{3z^2-r^2}$ and Co $3d_{e_g}$ states is less pronounced and the band-crossing is encountered in the immediate vicinity of the Fermi surface. A strain-induced change of the Brillouin-zone can influence the position of this crossing and thus show significant impact on the shape of the Fermi surface. This might be exploited to alter transport properties by applying external fields, such as mechanical stress.

The crossing of the 16th band results in a hexagonal rod-like shape of the Fermi surface (Fig. 4b), which is a pronounced feature of both compounds.^{16,17,30-32} Under a moderate compressive epitaxial strain of $\varepsilon = -4\%$, the extremal features of the 15th and 17th band of PtCoO₂ touch the Fermi surface and changes its topology significantly. This is depicted in Fig. 4a and Fig. 4d. The (blue) needle-type features outside the (orange) hexagonal rod evolve from the rising of the hole pocket in the 15th band, which is best seen at the L-point. At the same time, the 17th band approaches the Fermi level along Γ -F from above resulting in the (red) pills inside the hexagonal rods. According to its Pt-type band-character (not shown), we expect the 15th band to contribute predominantly to the in-plane conductivity. In turn, the 17th band shows a strong Co-character close to its minimum where the electron pocket forms and is consequently expected to increase the out-of-plane conductivity (see Sec. III C). While the faces of the hexagon formed by the 16th band are essentially dispersionless irrespective of the strain, we find bulb-like extrusions at its rounded corners. The extrusions are also present on the Fermi surface of PdCoO₂ and are again associated to a slight admixture of Co-states in band 16 along Γ -F.⁴⁴ In PtCoO₂, these features grow under compressive strain and eventually

touch the Brillouin zone boundary, while they become significantly flatter under tensile strain, in turn. This corresponds to a diminished band velocity component in z -direction. Tensile epitaxial strain is thus a suitable possibility to control the Pd/Pt-character of the 16th band and thus enhance the twodimensional nature of the electronic structure. In reverse, compressive strain can stimulate an electronic topological transition, which arises from the appearance of additional bands at the Fermi level and the 16th band touching the Brillouin zone boundary. In PdCoO₂, the distance between the Co- and Pd-states along Γ -F is significantly larger, which makes the electronic states at the Fermi level much less susceptible to strain. However, electron doping may provide an alternative way to bring the systems close to this instability and produce a Fermi surface of similar shape.⁴⁵

Based on experimental evidence, PtCoO₂ and PdCoO₂ were considered as weakly correlated oxides.⁴⁶ Furthermore, Ong *et al.*^{16,17} found a very good agreement between the first-principles electronic structure and experimental spectroscopy, which justifies the use of conventional GGA for the exchange and correlation part of the Hamiltonian. However, recently, Hicks *et al.* argued that static Coulomb repulsion in terms of a Hubbard model with an effective U -parameter on the Co $3d$ states improves the agreement with their de-Haas-van-Alphen data.⁴⁷ Therefore, we carried out additional GGA+ U calculations for PdCoO₂ and PtCoO₂ under a systematic variation of the effective Coulomb repulsion $U_{\text{eff}} = U - J$ on Co $3d$ from 0 (pure GGA) to 5 eV. The additional term mainly affects the bonding $3d$ Co t_{2g} states below E_F which move further down, while we observe only a minute shift in the position of the relevant Co e_g states, which are close to E_F . This separates occupied and unoccupied Co and O states further, but hardly affects the Pd-states at the Fermi surface, which are responsible for metallicity. Thus U_{eff} has only minor effect on the position of the Pt-dominated 15th band but larger values will eventually inhibit the crossing of the 17th band or shift it to larger strains.

It is worthwhile to note that the occurrence of the electronic topological transition is independent of the calculation method and likewise reproduced with VASP and Wien2k. Nevertheless, concerning the transport calculations we obtain slight differences between the codes. Interestingly, we find a closer agreement of the GGA results obtained from the Wien2k calculations with the VASP calculations for $U_{\text{eff}} = 1$ eV, rather than for the pure GGA, although the same exchange-correlation functional (PBE) was used in both cases. We ascribe this to the specific implementation of the Co PAW-potential employed in the VASP calculations, which apparently allows for a somewhat stronger interaction between Co and Pd states resulting in a slightly increased presence of residual Co-states at the Fermi-level compared to the full-potential calculations. For additional details see the supplementary information.⁴⁰

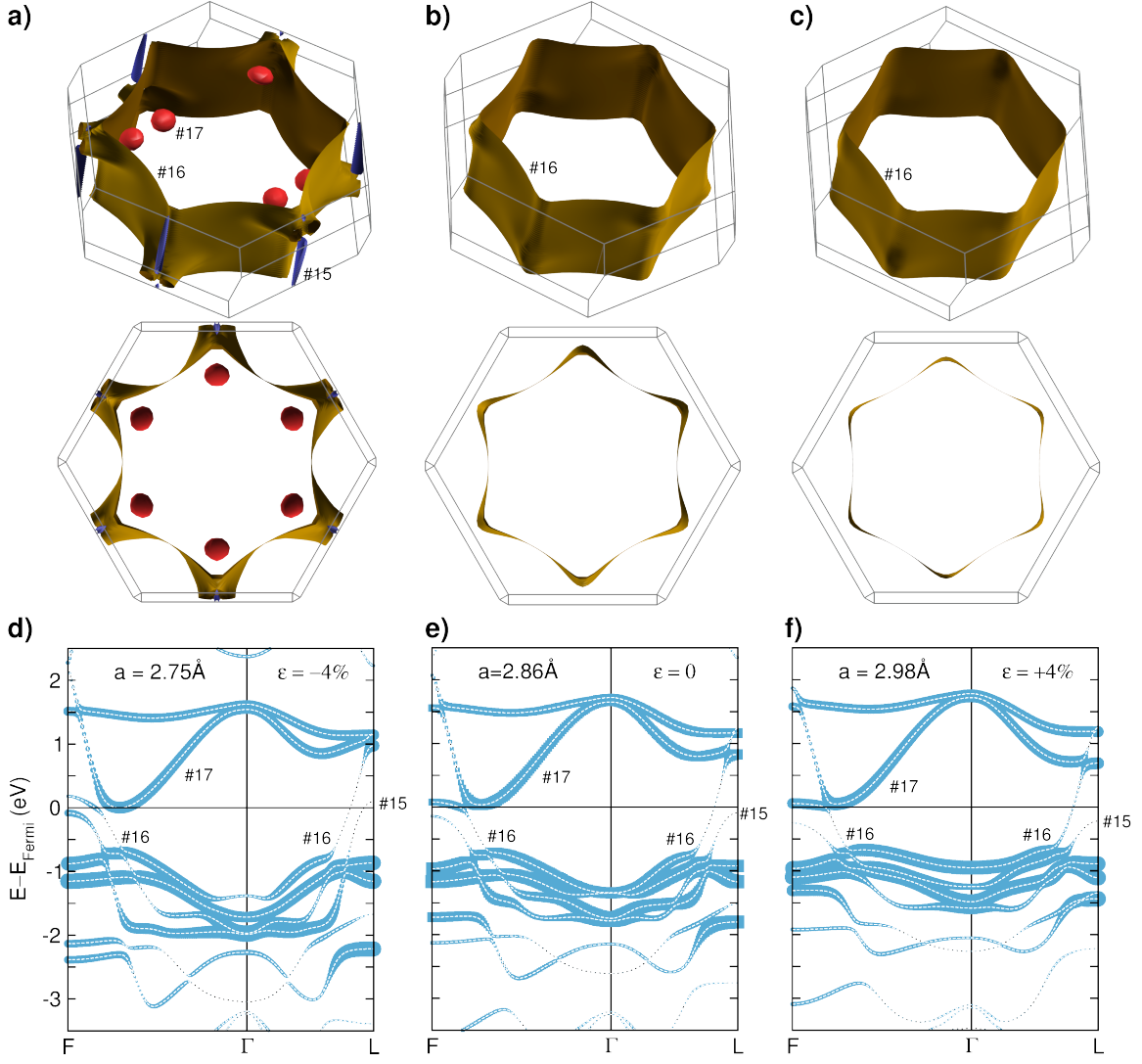


FIG. 4: (color online) Fermi surfaces (top and center rows, subfigures a-c) and corresponding band structure (bottom row, subfigures d-f) of strained and unstrained PtCoO_2 . The left column (subfigures a and d) refers to $\varepsilon = -4\%$ compressive epitaxial strain, the right column (subfigures c and f) to $\varepsilon = +4\%$ tensile strain and the center column (subfigures b and e) to the unstrained case. In the images of the Fermi surfaces the different colors refer to the different bands crossing the Fermi levels (blue: 15th band, orange: 16th band, red: 17th band). The vertical width of the (bright blue) fat bands in the bottom row is proportional to the Co-character of the band. Again, the bands crossing E_F are denoted by their respective number. We find that the 15th and 17th band cross the Fermi energy at compressive strains, whereas for tensile strains, the dispersion of the 16th band at E_F is influenced by the nearby crossing of a parabolic section of the 16th Pt-band and the 17th band which is dominated by Co states.

C. Electronic conductivity under epitaxial strain

Starting from the electronic eigenvalues obtained with DFT, we determined the transport properties in the framework of semi-classical Boltzmann transport theory using the constant relaxation time approximation. This approach has evolved as a standard tool for the prediction and identification of qualitative trends in a wide variety of materials,^{48,49} including the prediction of oxides systems,^{50,51} and has been applied successfully to several delafossites in the past.^{52,53} Concerning PdCoO_2 and

PtCoO_2 , particular emphasis was laid on the explanation of the large anisotropy in conductivity and thermopower (Seebeck coefficient),^{16,17,44} but also on the description of the large out-of-plane magnetoresistance encountered in PdCoO_2 under the rotation of a large in-plane magnetic field.⁵⁴ The relaxation time approximation, with a single energy- and momentum-independent relaxation time, assumes that the combined effect of all scattering processes is such that the electronic system relaxes back to equilibrium exponentially with a single time constant once the perturbation is switched off. Alternatively, one may con-

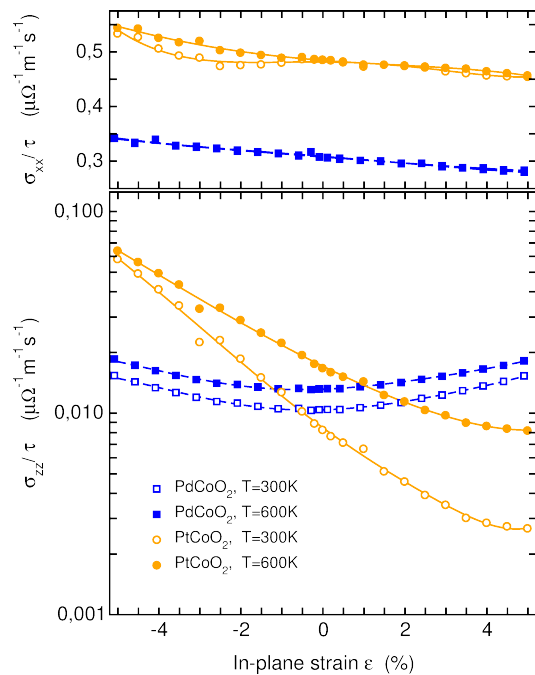


FIG. 5: (color online) In-plane and out of plane components of the electrical conductivity tensor, σ_{xx} (upper panel) and σ_{zz} (lower panel), as a function of epitaxial strain. The results are specified relative to the empirical parameter of Boltzmann transport theory, the relaxation time constant τ . We compare the two different compounds PdCoO₂ (dashed lines and squares) and PtCoO₂ (solid lines and circles) are compared at two different temperatures $T = 300$ K (open symbols) and $T = 600$ K (filled symbols). Please note the semi-logarithmic scale in the bottom panel.

sider this approach as a first step towards the complete description which clarifies the *band structure related* aspects of transport. In any case, the relaxation time approximation allows for solving the Boltzmann equation in a simple way, and hence an accurate determination of transport coefficients using 10^4 to 10^5 k -points, which are necessary for converged results. From the comparison with experiment, on the other hand, one is then able to deduce information on the relevant scattering mechanisms.

A more detailed theoretical description could be based on Boltzmann theory, but would require a first-principles calculation of phonon dispersions as well as electron-phonon scattering matrix elements, which is beyond the scope of the present work. Alternatively, the determination of transport coefficients could be based directly on a Green's function approach and Kubo's linear response theory (see Ref. 55 for a recent discussion).

At room temperature and above, it can be expected that electron-phonon scattering is the dominant relaxation mechanism. For the nearly-free electron model, the scattering operator indeed has been studied in detail.⁵⁶ For example, it is well known that for temperatures be-

low the Debye temperature, the momentum and energy relaxation rates are very different, the latter being much shorter than the former. Above the Debye temperature, electron-phonon scattering is essentially elastic, and both rates are very similar. These results rely, in particular, strongly on the fact that the electronic density of states (DOS) is practically independent of energy around the Fermi level. Thus predictions based on an energy-independent τ are likely to fail in case sharp features exist close to E_F . This was shown recently for the simple metal Li, where the constant relaxation time approximation predicts the wrong sign of the thermopower.⁵⁷ For Li, quantitative agreement can be achieved within a variational approach to Boltzmann theory.^{57–60} Since our calculated transport properties are consistent with the available experimental data for PdCoO₂, as shown below, we do not expect significant new insights from an advanced treatment of the Boltzmann equation. However, our results will demonstrate clearly that – according to the anisotropic nature of the lattice structure – one must take into account at least a directional dependence of τ in addition to its variation with temperature.

In practice, all transport tensors obtained from Boltzmann transport theory turn out to be essentially diagonal; there are only two distinct entries. The first, marked with the index “xx”, corresponding to in-plane transport, the second, marked as “zz” corresponding to transport properties perpendicular to the Co-O and Pd-O/Pt-O layers.

As already anticipated, the significant changes at the Fermi surface of PtCoO₂ should leave a corresponding signature in the strain-dependent conductivity, shown in Fig. 5. The variation of the in-plane conductivity, which accounts for the already very good conductivity in this direction, is not substantial (upper panel). According to the steeper slope at E_F , we find a larger ratio σ_{xx}/τ for PtCoO₂ compared to PdCoO₂. Both values are steadily reduced for tensile strains. However, as indicated earlier, the conductivity is highly anisotropic and thus orders of magnitude smaller in the perpendicular direction. According to the changes in the Fermi surface, the strain induced variation of the out-of-plane conductivity is much more significant for bulk PtCoO₂. Expanding the a -axis by 4% decreases the out-of-plane conductivity by almost one order of magnitude. In turn, the opposite trend is encountered for compressive strain. This significantly increases the conductivity compared to PdCoO₂, where the variations are much smaller and do not exhibit a consistent trend for both strain directions.

The strong impact of the Fermi surface on the conductivity anisotropy in PtCoO₂ is explained by the band resolved in-plane and out-of-plane components of the electrical conductivity tensor of PtCoO₂ (Fig. 6). We see that for tensile strains only the 16th band contributes since it is still the only one crossing the Fermi surface. Its in-plane component remains essentially constant, while the out-of-plane component is responsible for the exponential decrease of the conductivity anisotropy shown in

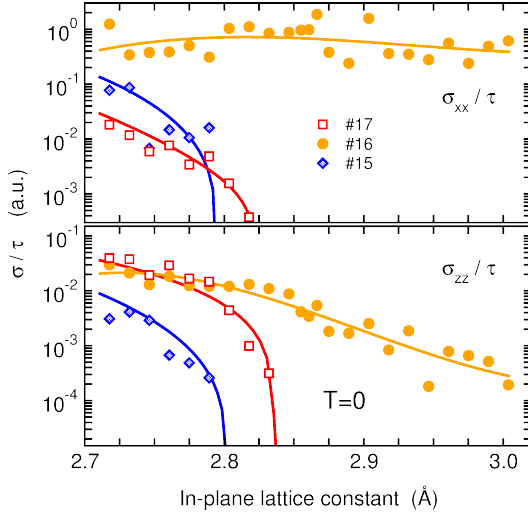


FIG. 6: (color online) Band-resolved diagonal components σ_{xx} and σ_{zz} of the electronic conductivity tensor at $T=0$ of PtCoO_2 as a function of the in-plane lattice constant a . The values are specified relative to the relaxation time constant τ . Only three bands crossing E_F contribute to the transport properties.

Fig. 5. The additional bands start contributing to the conductivity tensor below an in-plane lattice constant $a < 2.80 \text{ \AA}$ (15th band) and $a < 2.83 \text{ \AA}$ (17th band), respectively, see Fig. 6. For tensile strains, the conductivity is maintained by the 16th band, alone. Its strong decrease can be related to an increasingly better definition of the hexagonal corners of the Fermi-surface along the k_z , as visible from the comparison of the Fermi surface under tensile strain with the equilibrium Fermi surface (Fig. 4a-4c, center row). This corresponds to a diminished band velocity component in z -direction, which consequently reduces the respective element of the conductivity tensor. In a simple geometric picture, this complies with the decreasing width of the conducting PtO_2 -layer, while the separation between O and Co and thus the width of the insulating layer becomes larger.

Recent experiments obtained for the anisotropy σ_{xx}/σ_{zz} of PdCoO_2 values ranging from 150 (Ref. 43), 280 (Ref. 61) to 400 (Ref. 47). This large discrepancy has been noticed earlier and related to the treatment of umklapp processes and the anisotropy of defect scattering cross sections.⁴⁷ In particular, the latter aspects point out possible shortcomings of the single relaxation time approximation and semi-classical Boltzmann transport theory. Computing the anisotropy ratio from Fig. 5 assuming a single constant τ , the in-plane conductivity is a factor 30 larger than out-of-plane. This ratio can be somewhat increased by applying static Coulomb correlations within the GGA+ U scheme (see the supporting information⁴⁰ for more details) but it never becomes comparable to the experimental results. We take this as another indication that a directional dependence

of τ , which has been neglected so far, should enter the anisotropy ratio.

The diagonal structure of the transport tensors allows us to pragmatically circumvent this problem by introducing two effective, temperature dependent relaxation time constants for in-plane and out-of-plane processes, τ_{xx} and τ_{zz} , respectively, which we obtain by comparison with the experimental conductivities. This effectively reintroduces the k -vector dependence of τ , which is discarded in Boltzmann theory within the common single relaxation time approximation. As for the anisotropy, experiment offers a considerable span of results also for the in-plane experimental conductivities σ_{xx} , ranging from $14.5 \mu\Omega^{-1}\text{m}^{-1}$ (Ref. 43), over $32.3 \mu\Omega^{-1}\text{m}^{-1}$ (Ref. 61) and $38.5 \mu\Omega^{-1}\text{m}^{-1}$ (Ref. 47) to $50 \mu\Omega^{-1}\text{m}^{-1}$ (Ref. 12). This results in relaxation time constants $\tau_{xx}(300 \text{ K})$ of 46 fs, 101 fs, 121 fs and 157 fs, respectively. These comparatively large values are consistent with the previous assessment of Ong *et al.*,¹⁷ obtained in a similar fashion by comparing Boltzmann theory and experimental conductivity data. From the residual in-plane resistivities for $T \rightarrow 0$, Hicks *et al.*⁴⁷ concluded on an extremely large transport mean free path $l_{\text{MFP}} = 20 \mu\text{m}$. This is considerably larger than the earlier estimate $l_{\text{MFP}} = 60 \text{ \AA}$ of Noh *et al.*³² based on the peak width obtained from ARPES. These measurements also yield a value for the in-plane carrier velocity of $4.96 \text{ eV \AA}^{-1} \hbar^{-1}$ which is consistent with first-principles results.¹⁷ Thus, relaxation time constants obtained from experiment were either significantly smaller, such as the 7.6 fs estimated by Noh *et al.*³² or larger, based on the de-Haas-van-Alphen measurements of Hicks *et al.*⁴⁷ or the analysis of anomalous magnetoresistance.⁵⁴ For the out of plane direction, ambient σ_{zz} was measured as $0.096 \mu\Omega^{-1}\text{m}^{-1}$ (Ref. 47), $0.097 \mu\Omega^{-1}\text{m}^{-1}$ (Ref. 43) and $0.115 \mu\Omega^{-1}\text{m}^{-1}$ (Ref. 61), corresponding to $\tau_{zz}(300 \text{ K}) = 9 \text{ fs}$ and 11 fs , respectively, which yields a more uniform picture than the in-plane-case.

Most experiments were carried out at room temperature and below, only Takatsu *et al.* performed conductivity measurements up to 500 K. Thus, only Ref. 43 offers a reasonable possibility to extrapolate the experimental conductivities to $T=600 \text{ K}$. We find then $\sigma_{xx} = 5 \mu\Omega^{-1}\text{m}^{-1}$ and $\sigma_{zz} = 0.04 \mu\Omega^{-1}\text{m}^{-1}$, which corresponds to $\tau_{xx}(600 \text{ K}) = 16 \text{ fs}$ and $\tau_{zz}(600 \text{ K}) = 4 \text{ fs}$. For PtCoO_2 , Rogers *et al.*¹² reported conductivities $\sigma_{zz} = 33 \mu\Omega^{-1}\text{m}^{-1}$ and $\sigma_{xx} = 0.1 \mu\Omega^{-1}\text{m}^{-1}$. This leads to $\tau_{xx}(300 \text{ K}) = 70 \text{ fs}$ and $\tau_{zz}(300 \text{ K}) = 12 \text{ fs}$, which is fairly close to the relaxation times obtained for PdCoO_2 .

D. Thermoelectric performance

The thermopower of PdCoO_2 was first reported by Yagi *et al.*⁶² for temperatures above 500 K. Since the authors measured on polycrystalline materials, the highly anisotropic behavior of this quantity was overseen. Later, Hasegawa *et al.*⁶³ measured the thermopower at lower

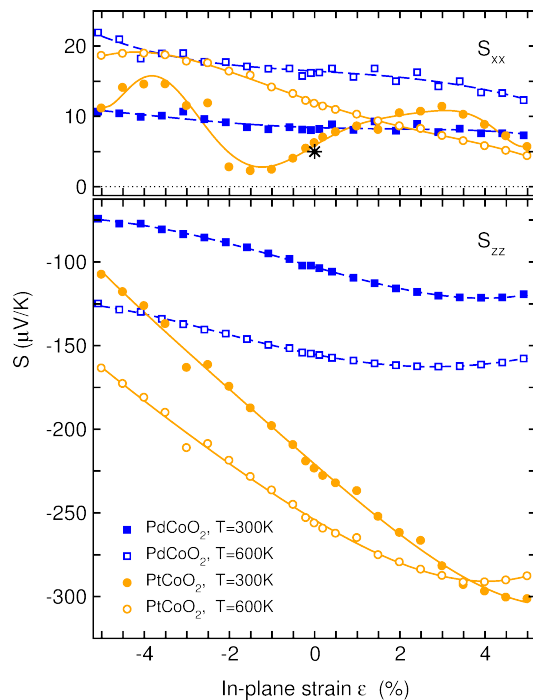


FIG. 7: (color online) Diagonal elements S_{xx} (upper panel) and S_{zz} (lower panel) of the tensorial thermopower of PdCoO_2 (blue dashed lines and squares) and PtCoO_2 (orange solid lines and circles) as a function of the epitaxial in-plane strain for two different temperatures $T = 300$ K (open symbols) and $T = 600$ K (filled symbols). The black star in the upper panel marks the experimental in-plane thermopower of PdCoO_2 at $T = 300$ K taken from Ref. 61.

temperatures, again on powdered and sintered crystals. The authors obtained a positive value of $S = 2 \dots 4 \mu\text{V K}^{-1}$ at room temperature, which is comparable to conventional metals. In a very recent study the in-plane thermopower S_{xx} and thermal conductivity of PdCoO_2 was measured for temperatures below 300 K.⁶¹ S_{xx} exhibits a change of sign below $T < 100$ K, but approaches the expected linear temperature dependence at higher temperatures, reaching $S_{xx} = 5 \mu\text{V K}^{-1}$ at ambient conditions.

Fig. 7 shows the calculated thermopower (Seebeck coefficient) S as a function of the epitaxial strain for both directions and two different temperatures $T = 300$ K and $T = 600$ K. For both systems, we confirm the marked anisotropy in the Seebeck coefficient, which is significantly more pronounced for PtCoO_2 than for PdCoO_2 and increases with temperature. It is positive for the in-plane component S_{xx} , which indicates a higher mobility of p-type carriers (holes), while large negative values for S_{zz} point out the dominance of n-type carriers (electrons) for transport in out-of-plane direction. The estimate for S_{xx} of unstrained PdCoO_2 from Boltzmann theory at room temperature is approximately 1.6 times larger than the experimental value published in Ref. 61. This might still be considered a reasonable agreement

keeping in mind the simplifications of Boltzmann transport theory and experimental difficulties in obtaining this quantity. Previous calculations by Ong *et al.*^{16,17} report moderate positive values in-plane for S_{xx} , while the out of plane component S_{zz} provides a large negative contribution. Our values compare well to the results of Ong *et al.*,¹⁷ who carried out their calculations with the Wien2k code for the experimental lattice constant, which differs slightly from our setup.

We now turn to the effect of strain, which is varied from -5% compressive to +5% tensile strain. The in-plane thermopower S_{xx} and its variation under strain remains moderate in absolute numbers. We achieve changes in the range of 10...12 $\mu\text{V/K}$ at $T = 600$ K as compared to $\varepsilon = 0$ for both systems. Nevertheless, as the absolute values are small, maximum strain corresponds to a relative change by a factor of two for the Pt-based oxide. The oscillations observed at lower temperatures are a consequence of the electronic topological transition related to the two additional bands consecutively crossing the Fermi level. For the out-of-plane component S_{zz} , we find much larger changes in absolute numbers, in particular, around room temperature. Here, the tensile strain yields a relative increase of 60% to 180%, which corresponds to rather significant changes in absolute numbers of -47 $\mu\text{V/K}$ and -196 $\mu\text{V/K}$ for PdCoO_2 than for PtCoO_2 , respectively.

In particular, for PtCoO_2 , the variation of the out-of-plane thermopower, S_{zz} , with strain bears close similarities with the logarithm of the strain dependence of the conductivity element σ_{zz} . Such a relation is motivated by the textbook formula of Mott, which connects the scalar thermopower S of an isotropic system with the logarithmic derivative of the (scalar) conductivity σ with respect to the chemical potential μ :

$$S = \frac{\pi^2 k_B^2 T}{3e} \frac{\partial}{\partial \mu} \ln[\sigma(\mu)], \quad (1)$$

We therefore conclude that the large strain variations in the thermopower originate from the corresponding changes in the conductivity discussed above. The negative sign of S_{zz} is related to the decrease of σ_{zz} with increasing chemical potential μ at a given strain,⁴⁴ while the strong variation of the magnitude of $|S_{zz}|$ with strain relates inversely to the change in conductivity.

The figure of merit of a material with respect to its thermoelectric performance is given by the dimensionless number $ZT = S^2 \sigma T / (\kappa^{\text{el}} + \kappa^{\text{ph}})$, where κ^{el} and κ^{ph} are the electronic and lattice thermal conductivity, respectively. Apart from κ^{ph} , all quantities are accessible within our approach. However, κ^{ph} becomes the dominant contribution, when the electrical conductivity is minute, e.g. in semiconductors or insulators, and will thus be relevant for the out-of-plane transport. The calculation of κ^{ph} from first-principles requires the determination of the anharmonic contributions to lattice dynamics, which is beyond the scope of the present work. However, the total and lattice contributions to the thermal conductivity of PdCoO_2 were recently obtained experi-

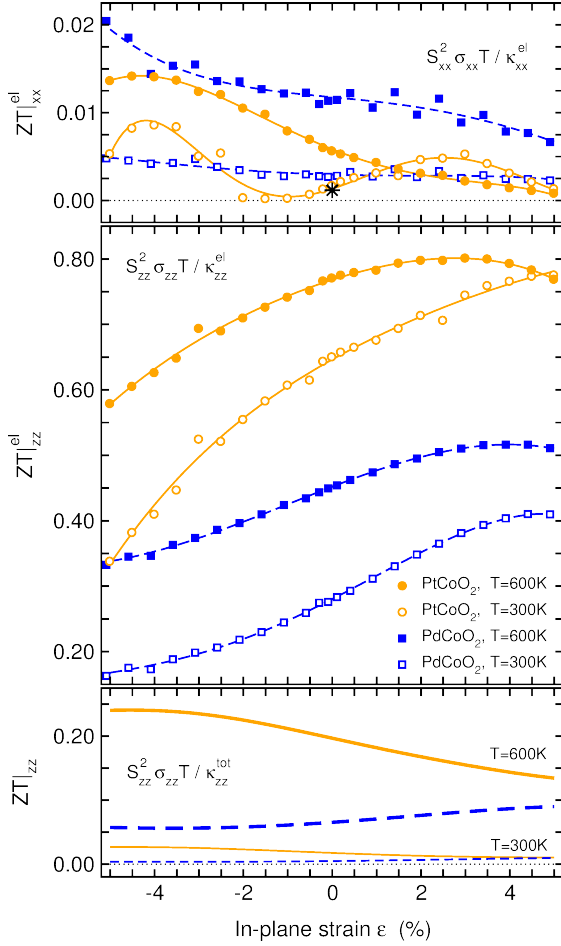


FIG. 8: (color online) Thermoelectric figure of merit, ZT , calculated from the diagonal elements of the transport tensors (upper panel, xx elements; lower panel zz elements, symbols and colors as in the preceding figures). Thin lines and data points in the upper and midel panel denote an upper boundary ZT^{el} as lattice thermal conductivity is neglected. The bottom panel shows an estimate of the total ZT using the experimental κ_{zz}^{ph} for PdCoO₂ from Ref. 61 (see text) and the relaxation time constant $\tau = 10$ fs (same values for both compounds and all strains). The thin lines refer to $T = 300$ K and the thick lines to $T = 600$ K, while broken lines denote PdCoO₂ and solid lines PtCoO₂. The black star in the upper panel marks the experimental in-plane ZT of PdCoO₂ at $T = 300$ K calculated from the experimental data of Daou and coworkers.⁶¹

mentally by Daou *et al.*⁶¹ for temperatures up to 320 K. For the in-plane case, the authors reported a rather large total thermal conductivity κ_{xx}^{tot} of $250 \text{ W K}^{-1} \text{ m}^{-1}$, while the total out-of-plane conductivity κ_{zz}^{tot} amounts to approximately $70 \text{ W K}^{-1} \text{ m}^{-1}$ at ambient conditions. According to the Wiedemann-Franz law, the electronic contribution κ_{zz}^{el} is expected to be at least one order of magnitude smaller, based on the very low out-of-plane conductivity. This yields thus a direct estimate of the lattice thermal conductivity κ_{zz}^{ph} .

According to the Wiedemann-Franz law, the electronic conductivities κ^{el} increase with temperature, whereas for the lattice thermal conductivity κ^{ph} a fast decrease is expected according to the Debye-Callaway model. For the in-plane component of ZT , we can neglect κ^{ph} as a first approximation since it is significantly exceeded by κ^{el} . The corresponding quantity, which we denote by ZT^{el} , provides thus an upper limit for the true ZT . According to the large thermal conductivity, the in-plane values turn out to be prohibitively low from the application point of view. Since the strain dependence of σ and κ^{el} essentially cancels out, the strain dependence of ZT^{el}_{xx} is dominated by the contribution from S_{xx}^2 (cf. Fig. 8). This is also the case for ZT^{el}_{zz} . However, since the thermal conductivity is dominated by the lattice contribution, we cannot use ZT^{el}_{zz} to assess the thermoelectric performance of the material. Instead, we determine the complete ZT_{zz} with the help the experimental value κ_{zz}^{ph} of Ref. 61 for $T = 300$ K and $\kappa_{zz}^{\text{ph}} = 10 \text{ W K}^{-1} \text{ m}^{-1}$ for $T = 600$ K, which can be estimated from the fit to the Debye-Callaway model provided in Ref. 61. In addition, we use an average $\tau_{zz} = 10$ fs for $T = 300$ K, while for $T = 600$ K, we take $\tau_{zz} = 4$ fs, as discussed in Sec. III C. As there is only sufficient data for PdCoO₂, we use the same parameters for both systems. The strain dependence of ZT_{zz} is plotted as thick dashed (PdCoO₂) and solid (PtCoO₂) lines in the bottom part of Fig. 8. Since the dominant contribution to thermal conductivity comes from the lattice, which we assume constant for all ε , the strain dependence of ZT_{zz} rather resembles the power factor (see supplementary information⁴⁰). As a general trend, we see that ZT_{zz} increases strongly with temperature, while PtCoO₂ clearly exceeds the performance of PdCoO₂. Thus, only PtCoO₂ can reach a reasonable figure of merit of $ZT_{zz} = 0.25$ at compressive epitaxial strains and sufficiently high temperatures, which is a consequence of the electronic topological transition.

IV. CONCLUSIONS

Based on first-principles calculations in combination with Boltzmann transport theory in the single relaxation time approximation, we provide a systematic analysis of the electronic structure and anisotropic transport properties of the delafossites PdCoO₂ and PtCoO₂ under epitaxial strain. We demonstrate that despite the large similarities in both systems concerning their structural properties that PtCoO₂ has – unlike PdCoO₂ – the propensity to undergo an electronic topological transition, which might be triggered by a realistic compressive epitaxial strain. In turn, by expanding the in-plane lattice constant, it exhibits a dimensional crossover from a three-dimensional open Fermi surface, which touches the zone boundary in-plane and out of plane, to a nearly perfect twodimensional electronic system, with a closed hexagonal Fermi-surface with perfectly flat sides extending in k_z -direction.

Comparing the in-plane and out-of-plane conductivities from our calculations based on GGA correlation and the GGA+ U approach with experiment, we propose that two different relaxation times must be introduced to describe in-plane and out-of-plane transport appropriately in Boltzmann transport theory. We consider this approach justified in the present case due to the essentially diagonal structure of the transport tensors.

We finally predict that, despite the apparent similarities of both oxides, PtCoO₂ exhibits a much better thermoelectric performance than PdCoO₂ and might thus be a better model system for applications. Our analysis includes the thermoelectric figure of merit ZT , which we obtain by combining theoretical results with recently available experimental data for the lattice thermal conductivity of PdCoO₂.⁶¹ The presence of the topological transition significantly helps in improving this number, since it increases the out-of-plane conductivity, which can be tuned efficiently by an external control parameter, such as epitaxial strain. In this way, we can balance the contributions of electronic and lattice thermal conductivity effectively, while still allowing for sufficiently large absolute values of the thermopower. With this strategy we arrive at a reasonable figure of merit of $ZT = 0.25$ at $T = 600$ K in out-of-plane direction for a system under compressive in-plane strain. For tensile strains the out-

of-plane conductivity becomes very low and ZT small, since the lattice thermal conductivity dominates. But since the thermopower is almost three times larger than for compressive strains, appropriate doping of carriers may still improve the thermoelectric performance reasonably.

In conclusion, the results for PtCoO₂ as a model system confirm that metallic materials characterized by a quasi-twodimensional Fermi surface may be well suited for thermoelectric applications. However, we emphasize that for a reasonable performance the two-dimensional shape must not be too perfect. In the present case, epitaxial strain was used effectively as an external parameter to obtain a certain level of imperfection that optimizes the relation of electrical and thermal conductivities in the figure of merit.

Acknowledgments

The authors gratefully acknowledge useful discussions with H.-U. Haberman, B. Keimer (Stuttgart) and M. Verstraete (Liège). Financial support was granted by the Deutsche Forschungsgemeinschaft in the framework of SFB/TRR 80 (project G8).

-
- * Electronic address: Markus.Gruner@uni-due.de
- ¹ C. Wood, Rep. Prog. Phys. **51**, 459 (1988).
 - ² G. J. Snyder and E. S. Toberer, Nature Mater. **7**, 105 (2008).
 - ³ L. D. Hicks and M. S. Dresselhaus, Phys. Rev. B **47**, 12727 (1993).
 - ⁴ R. Venkatasubramanian, E. Siivola, T. Colpitts, and B. O'Quinn, Nature **413**, 597 (2001).
 - ⁵ P. F. P. Poudeu, J. D'Angelo, A. D. Downey, J. L. Short, T. P. Hogan, and M. G. Kanatzidis, Angew. Chem. Int. Ed. **45**, 3835 (2006).
 - ⁶ H. Ohta, S. Kim, Y. Mune, T. Mizoguchi, K. Nomura, S. Ohta, T. Nomura, Y. Nakanishi, Y. Ikuhara, M. Hirano, et al., Nature Mater. **6**, 129 (2007).
 - ⁷ I. Terasaki, Y. Sasago, and K. Uchinokura, Phys. Rev. B **56**, R12685 (1997).
 - ⁸ K. Fujita, T. Mochida, and K. Nakamura, Jpn. J. Appl. Phys. **40**, 4644 (2001).
 - ⁹ M. Shikano and R. Funahashi, Appl. Phys. Lett. **82**, 1851 (2003).
 - ¹⁰ K. Koumoto, I. Terasaki, and R. Funahashi, MRS Bulletin **31**, 206 (2006).
 - ¹¹ J. He, Y. Liu, and R. Funahashi, J. Mater. Res. p. 1762 (2011).
 - ¹² D. B. Rogers, R. D. Shannon, C. T. Prewitt, and J. L. Gillson, Inorg. Chem. **10**, 723 (1971).
 - ¹³ R. Nagarajan, N. Duan, M. K. Jayaraj, J. Li, K. A. Vanaja, A. Yokochi, A. Draeseke, J. Tate, and A. W. Sleight, Int. J. Inorg. Mater. **3**, 265 (2001).
 - ¹⁴ M. A. Marquardt, N. A. Ashmore, and D. P. Cann, Thin Solid Films **496**, 146 (2006).
 - ¹⁵ M. Tanaka, M. Hasegawa, and H. Takei, J. Phys. Soc. Jpn **65**, 3973 (1996).
 - ¹⁶ K. P. Ong, J. Zhang, J. S. Tse, and P. Wu, Phys. Rev. B **81**, 115120 (2010).
 - ¹⁷ K. P. Ong, D. J. Singh, and P. Wu, Phys. Rev. Lett. **104**, 176601 (2010).
 - ¹⁸ G. W. Yan, L. Yu, Y. Wang, H. Zhang, P. X. Zhang, and H.-U. Haberman, J. Appl. Phys. **110**, 103102 (2011).
 - ¹⁹ R. D. Shannon and C. T. Prewitt, J. Inorg. Nucl. Chem. **32**, 1427 (1970).
 - ²⁰ R. D. Shannon, D. B. Rogers, and C. T. Prewitt, Inorg. Chem. **10**, 713 (1971).
 - ²¹ C. Prewitt, R. Shannon, and D. Rogers, Inorg. Chem. **10**, 719 (1971).
 - ²² M. Tanaka, M. Hasegawa, and H. Takei, J. Crystal Growth **173**, 440 (1997).
 - ²³ M. Tanaka, M. Hasegawa, T. Higuchi, T. Tsukamoto, Y. Tezuka, S. Shin, and H. Takei, Physica B **245**, 157 (1998).
 - ²⁴ T. Higuchi, D. Baba, Y. Yokoyama, M. Hasegawa, M. Tanaka, H. Takei, and A. Fukushima, Jpn. J. Appl. Phys. **42**, 5698 (2003).
 - ²⁵ T. Higuchi, M. Hasegawa, M. Tanaka, H. Takei, S. Shin, and T. Tsukamoto, Jpn J. Appl. Phys. **43**, 699 (2004).
 - ²⁶ H.-J. Noh, J. Jeong, J. Jeong, H. Sung, K. J. Park, J.-Y. Kim, H.-D. Kim, S. B. Kim, K. Kim, and B. I. Min, Phys. Rev. B **80**, 073104 (2009).
 - ²⁷ T. Higuchi, T. Tsukamoto, M. Tanaka, H. Ishii, K. Kanai, Y. Tezuka, S. Shin, and H. Takei, J. Electron Spectroscopy **92**, 71 (1998).
 - ²⁸ M. Hasegawa, T. Higuchi, M. Tanaka, T. Tsukamoto,

- S. Shin, and H. Takei, *Mater. Trans.* **42**, 961 (2001).
- ²⁹ R. Seshadri, C. Felser, K. Thieme, and W. Tremel, *Chem. Mater.* **10**, 2189 (1998).
- ³⁰ V. Eyert, R. Fresard, and A. Maignan, *Chem. Mater.* **20**, 2370 (2008).
- ³¹ K. Kim, H. C. Choi, and B. I. Min, *Phys. Rev. B* **80**, 035116 (2009).
- ³² H.-J. Noh, J. Jeong, J. Jeong, E.-J. Cho, S. B. Kim, K. Kim, B. I. Min, and H.-D. Kim, *Phys. Rev. Lett.* **102**, 256404 (2009).
- ³³ G. Kresse and J. Furthmüller, *Phys. Rev. B* **54**, 11169 (1996).
- ³⁴ G. Kresse and D. Joubert, *Phys. Rev. B* **59**, 1758 (1999).
- ³⁵ P. E. Blöchl, *Phys. Rev. B* **50**, 17953 (1994).
- ³⁶ J. P. Perdew, K. Burke, and M. Ernzerhof, *Phys. Rev. Lett.* **77**, 3865 (1996).
- ³⁷ P. Blaha, K. Schwarz, G. K. H. Madsen, D. Kvasnicka, and J. Luitz, *WIEN2k, an augmented plane wave + local orbitals program for calculating crystal properties*, Karlheinz Schwarz, Techn. Universität Wien, Austria (2001), ISBN 3-9501031-1-2.
- ³⁸ G. K. H. Madsen and D. J. Singh, *Comput. Phys. Commun.* **175**, 67 (2006).
- ³⁹ S. L. Dudarev, G. A. Botton, S. Y. Savrasov, C. J. Humphreys, and A. P. Sutton, *Phys. Rev. B* **57**, 1505 (1998).
- ⁴⁰ See *supplementary material at*, URL [URLwillbeinsertedbypublisher](#).
- ⁴¹ S. Kumar, H. C. Gupta, and Karandeep, *J. Phys. Chem. Solids* **74**, 305 (2013).
- ⁴² M. Hasegawa, M. Tanaka, T. Yagi, H. Takei, and A. Inoue, *Solid State Commun.* **128**, 303 (2003).
- ⁴³ H. Takatsu, S. Yonezawa, S. Muori, S. Nakatsui, K. Tanaka, and Y. Maeno, *J. Phys. Soc. Jpn.* **76**, 104701 (2007).
- ⁴⁴ K. Kim, J. Kim, and B. Il Min, *J. Phys. Soc. Jpn* **83**, 124708 (2014).
- ⁴⁵ C. Felser, K. Thieme, and R. Seshadri, *J. Mater. Chem.* **9**, 451 (1999).
- ⁴⁶ M. Itoh, M. Mori, M. Tanaka, and H. Takei, *Physica B* **259**, 999 (1999).
- ⁴⁷ C. W. Hicks, A. S. Gibbs, A. P. Mackenzie, H. Takatsu, Y. Maeno, and E. A. Yelland, *Phys. Rev. Lett.* **109**, 116401 (2012).
- ⁴⁸ T. J. Scheidemantel, C. Ambrosch-Draxl, T. Thonhauser, J. V. Badding, and J. O. Sofo, *Phys. Rev. B* **68**, 125210 (2003).
- ⁴⁹ L. Bjerg, G. K. H. Madsen, and B. B. Iversen, *Chem. Mater.* **23**, 3907 (2011).
- ⁵⁰ P. Delugas, A. Filippetti, M. J. Verstraete, I. Pallecchi, D. Marré, and V. Fiorentini, *Phys. Rev. B* **88**, 045310 (2013).
- ⁵¹ G. B. Wilson-Short, D. J. Singh, M. Fornari, and M. Szwed, *Phys. Rev. B* **75**, 035121 (2007).
- ⁵² D. J. Singh, *Phys. Rev. B* **76**, 085110 (2007).
- ⁵³ A. Maignan, V. Eyert, C. Martin, S. Kremer, R. Frésard, and D. Pelloquin, *Phys. Rev. B* **80**, 115103 (2009).
- ⁵⁴ H. Takatsu, J. J. Ishikawa, S. Yonezawa, H. Yoshino, T. Shishidou, T. Oguchi, K. Murata, and Y. Maeno, *Phys. Rev. Lett.* **111**, 056601 (2013).
- ⁵⁵ H. Ebert, D. Ködderitzsch, and J. Minaár, *Rep. Prog. Phys.* **74**, 096501 (2011).
- ⁵⁶ J. M. Ziman, *Electrons and Phonons*, Oxford University Press, Oxford, 1960.
- ⁵⁷ B. Xu and M. Verstraete, *Phys. Rev. Lett.* **112**, 196603 (2014).
- ⁵⁸ P. B. Allen, *Phys. Rev. B* **17**, 3725 (1978).
- ⁵⁹ S. Y. Savrasov and D. Y. Savrasov, *Phys. Rev. B* **54**, 16487 (1996).
- ⁶⁰ B. Xu and M. Verstraete, *Phys. Rev. B* **87**, 134302 (2013).
- ⁶¹ R. Daou, R. Frésard, S. Hébert, and A. Maignan, *Phys. Rev. B* **91**, 041113 (2015).
- ⁶² H. Yagi, W.-S. Seo, and K. Koumoto, *Key Eng. Mater.* **181-182**, 63 (2000).
- ⁶³ M. Hasegawa, I. Inagawa, M. Tanaka, I. Shirogami, and H. Takei, *Solid State Commun.* **121**, 203 (2002).